THERMAL STRESS ANALYSIS OF PCM CONTAINERS FOR TEMPERATURE SMOOTHING OF WASTE GAS

F. Dal Magro, D. Benasciutti, G. Nardin

University of Udine – Department of Electrical, Management and Mechanical Engineering

Via delle Scienze 208 – 33100 Udine, e-mail: dalmagro.fabio@spes.uniud.it

Abstract

This article develops an analytical and numerical approach to evaluate thermal stress in a phase change material (PCM) system, used for temperature smoothing of waste gas of Electric Arc Furnace, in which the PCM is encapsulated in a cylindrical steel container. Thermal analysis shows that temperature distribution in the PCM system can be considered as uniform at any time instant according to the lumped capacitance method; the thermal behaviour of PCM system is thus simulated as a sequence of steady state analyses. Mechanical analysis adopts an axialsymmetric plane analytical model to compare elastic thermal stress distribution for different stainless steels and to identify AISI 316 as the most suitable material for the PCM container. A simple two-bars model and a stress index are also used to allow a physical understanding and a satisfactory interpretation of the PCM system response. Mechanical analysis shows that thermal stresses exceed the yield point of both stainless steels used in the container. A finite element elastic-plastic model is then developed to estimate the extension of the plastic zone. Finally, an alternative PCM system geometry based on concentric pipes is designed to keep the maximum stresses in the PCM container below the yielding point. A sensitivity analysis shows that the most relevant design parameters of the alternative geometry are the diameter of inner pipe and thickness of the external pipe.

Keywords: Energy Recovery, Electric Arc Furnace, Phase Change Material (PCM), Thermal Stresses

Nomenclature

Acronyms

AISI	American Iron and Steel Institute
EAF	Electric Arc Furnace
FEM	Finite element method
PCM	Phase Change Material

Latin letters

A	area [m^2]
Bi	Biot number [-]
D	outer diameter [mm]
d	inner diameter [mm]
e	emissivity [-]
E	Elastic modulus [GPa]
H	latent heat [kJ/kg]
h	heat transfer coefficient [W/m^2K]
i	stress index [-]
k	Boltzmann Constant [W/m^2K^4]
L	characteristic length [m]
R	thermal resistance [m^2K/W]
r	radial coordinate [m]
T	temperature [°C]
t	thickness [mm]
u	displacement [mm]
z	axial coordinate [m]

Greek letters

α	thermal expansion coefficient [K^{-1}]
Γ	time instant [s]
Δ	property difference
ε	strain [-]
λ	thermal conductivity [W/m K]
μ	friction coefficient [-]
ν	Poisson ratio [-]
ξ	Elastic modulus ratio [-]
ρ	density [kg/m^3]
χ	radiation dampening factor [-]
σ	stress [MPa]
τ	shear stress [MPa]
ψ	thermal expansion ratio [-]

Subscript

A	aluminium bar
a	aluminium
av	average
conv	convection
crit	critical
e	external pipe
ext	external
f	fracture
g	waste gas
i	inner side
if	interface
int	internal
m	melting
max	maximum
mec	mechanical
o	outer side
r	radial
rad	radiation
ref	reference
rp	reduction pipe
S	steel bar
s	steel
th	thermal
tot	total
gtr	Guest-Tresca
vm	Von Mises
y	yielding
θ	tangential
z	axial

1. INTRODUCTION

Heat recovery in energy intensive industries, especially in steel industry, is gaining an increasing attention due to the energy policy of the European Union and the global economic context. In particular, heat recovery in steel industry represents one of the greatest opportunity to reduce the consumption of primary energy while increasing the competitiveness of the steelmaking business [1].

Electric Arc Furnace (EAF), one of the most employed technology for steelmaking, generates large amounts of waste gases. The thermal energy owned by the waste gases represents about 15% to 35% of the total energy provided to the steelmaking process [2].

The most common heat recovery system from waste gas involves pre-heating of metal scrap; however, its diffusion is mainly limited by problems related to dioxins formation [3].

In the last years, new approaches of heat recovery based on steam production (e.g. in [4] and [5]) have been developed to overcome the environmental issues caused by scrap pre-heating. The efficiency of heat recovery by steam production is limited, however, by the high variability of temperature and flow rate of the waste gas. During the steelmaking process, the waste gas temperature at settling chamber inlet (see Figure 1a) generally shows a fluctuation within a wide range, e.g. from 100°C to 1000°C in tens of minutes. These operative conditions make difficult to size a direct contact heat exchanger, even by taking into account oversizing and appropriate control systems.

A possible solution to smooth the variability of waste gas temperature is to exploit aluminium as a phase change material (PCM) [6]. The PCM device designed in [6] is formed by a set of PCM systems, in which aluminium is encapsulated in a steel cylinder in direct contact with the surrounding waste gas. The PCM systems are vertically aligned and hung to the rooftop of the settling chamber by an appropriate hooking system (see Figure 1a). The outer surface of each PCM system is then subjected to a corrosive environment and to a thermal load, which is mainly due to convection from waste gas.

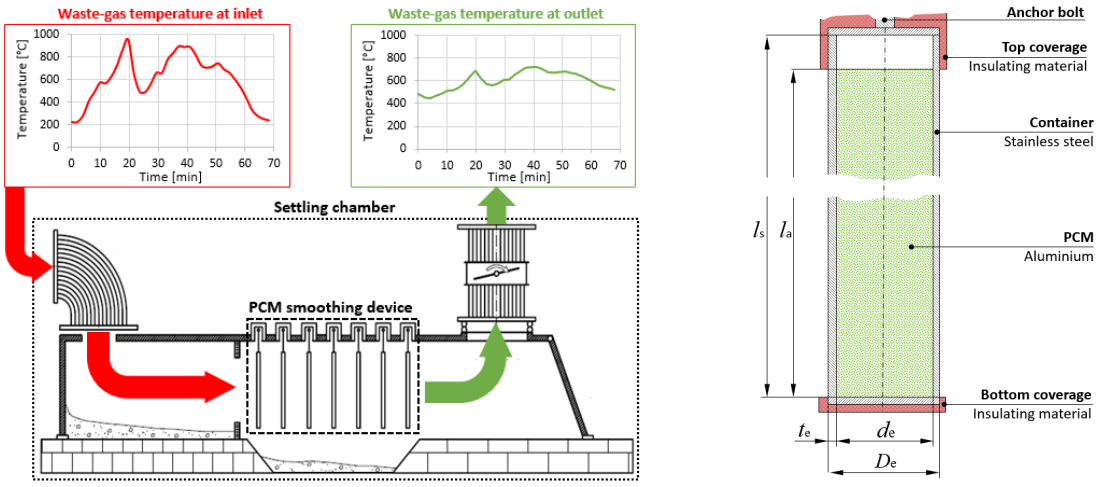

(a) (b)

Figure 1. (a) PCM-smoothing device and (b) geometry of the PCM system

The PCM system is then exposed to thermal loads that vary during the steelmaking process. The thermal expansion coefficient of the contained aluminium is higher than that of the containment material; this mismatch then gives rise to thermal stresses in the PCM container, which can affect its structural integrity.

To the author's knowledge, design procedures and regulations specifically dedicated to high-temperature applications of this kind of components (cylindrical geometry and PCM expansion in solid

phase) are not available in the literature. Some examples available in literature analyse expansion of PCM in liquid phase usually in spherical containers [7]-[8] and rarely in cylindrical container [9]. This work then aims to propose a simplified methodology for the thermo-mechanical analysis of a PCM system when in solid state, which would also allow identifying the most relevant design parameters for subsequent experimental validation. The thermo-structural behaviour of the PCM container is then investigated by a simple analytical thermo-elastic model, followed by an elasto-plastic finite element approach. A simple two-bars model and a stress index are also derived, to allow a physical understanding and a satisfactory interpretation of the PCM system response. This simplified methodology has been privileged over a more complex modelling approach, as it allows the obtained results to be directly used in the design.

After a short description of the PCM system, the article describes the analytical and numerical model used to study its thermo-mechanical behaviour. Finally, an alternative design that improves the structural thermo-mechanical behaviour is proposed.

2. THE PCM SYSTEM

The PCM smoothing device is based on the phase change phenomenon, which for pure materials and eutectic alloys occurs with a heat exchange at constant temperature (i.e. the phase change temperature). When the waste gas temperature is greater than the phase change temperature, the PCM absorbs heat from waste gas, whose temperature then decreases. At the opposite, waste gas temperature increases when it is lower than phase change temperature (the PCM then releases heat). The combination of these two effects leads to a smoothing of waste gas temperature, which tends to stabilise at the phase change temperature. The temperature-smoothing effect becomes as more effective as the average temperature of the waste gas (about 600°C) is closer to the phase change temperature, which then becomes one criterion to choose the PCM.

Other thermo-physical properties of PCM (e.g. latent heat of fusion and thermal conductivity) have also to be considered as choice criteria. A high latent heat of fusion is desirable to increase the energy storage capacity of the PCM system, while a high thermal conductivity assures a fast response to waste gas temperature variation.

To summarise, the best PCM should have a high latent heat, high thermal conductivity and a melting point close to waste gas temperature. These criteria identify the aluminium as the best candidate for PCM, as it has the melting point ($T_{m,a}$ = 660 °C) close to the average waste gas temperature ($T_{av,g}$ = 600°C), a high latent heat of fusion (H_a = 396 kJ/kg) and a high thermal conductivity (λ_a = 211 W/m K). In the PCM system, the PCM material is encapsulated by a steel container, see Figure 1b. A PCM device is composed by a set of PCM systems vertically aligned and hung to the rooftop of the settling chamber by an appropriate hooking system, as shown in Figure 1a. The hooking system allows the containers to oscillate in order to prevent accumulation of dust, which could hamper the waste gas flow. Table 1 reports the main characteristics of the component shown in Figure 1b.

Table 1. Geometric parameters of the PCM system

Outer diameter, D_e (mm)	60.3
Inner diameter, d_e (mm)	52.3
Thickness, t_e (mm)	4.0
Container length, l_s (m)	3.2
PCM length, l_a (m)	3.0

In the PCM device, all PCM systems are in direct contact with the surrounding waste gas; thus, they are subjected to thermal loads, corrosion (due to combination of high temperature and high concentration of chlorine compounds) and erosion (due to the high concentration of dust). In order to prevent overheating, the top and the bottom of the PCM container are protected by a coverage of insulating material, as sketched in Figure 1b. As reported in [6], the bottom coverage hampers the generation of a thermal bridge between the external wall and the bottom of the container. The presence of corrosive compounds in the settling chamber and the high temperature of the waste gas suggest the use of stainless steel as the most suitable material for the PCM container. Among available steel grades, two candidates have been identified: austenitic (AISI 316) and ferritic (AISI410S) stainless steel. Their temperature-dependent mechanical properties can be found in Eurocode 3 [10] and are listed in Table 3. Such stainless steels have differences in elastic modulus E and coefficient of thermal expansion α, which affect in a different way the thermal stresses generated in the PCM system. The stainless steel that is most suitable as PCM container will be identified by the analytical model developed in Section 4. The typical duty cycle of the PCM system is characterised by a start-up phase where the PCM temperature

increases, a running phase where phase change occurs, followed by a switch-off phase where the PCM system is brought back to room temperature.

Table 2. Thermo-physical properties of PCM system and waste gas

PCM – Aluminium	
Thermal conductivity (Solid State), λ_a (W/mK)	211
Melting temperature, $T_{m,a}$ (°C)	660
Latent heat of fusion, H_a (kJ/kg)	396
Density, ρ_a (kg/m^3)	2750
Container – Stainless Steel	
Thermal conductivity, λ_s (W/mK)	17
Density, ρ_s (kg/m^3)	7810
Waste gas	
Reference temperature, T_{ref} (°C)	20
Average temperature, $T_{av,g}$ (°C)	600
Convective heat transfer coefficient, h_{conv} (W/m^{2}K)	50÷100

During the start-up phase, the PCM system is heated from room temperature up to the melting point of the contained aluminium. During this phase, the aluminium always remains at solid state. Since the coefficient of thermal expansion of the steel container is lower than that of the PCM (Table 3), it is expected that the maximum stresses in the PCM container will be generated during the start-up phase, which will be then investigated in the next Sections.

During the running phase, instead, the PCM is subjected to phase change (melting or solidification); the coexistence of both liquid and solid states leads to a drastic reduction of PCM mechanical properties (in fact, the PCM in liquid state has almost null mechanical properties). Therefore, the mechanical stresses in the steel container are very small, as they are only due to gravity effects (i.e. the weight of PCM and steel container) and metallostatic pressure.

Finally, the mechanical response of the PCM system during the switch-off phase, when the PCM system comes back to solid state, is almost similar to the start-up phase.

The real temperature trends in Figure 1a, which lead to melting of PCM, suggest that the thermo-mechanical response of the PCM system should be studied by a transient analysis with phase change. From one hand, this modelling would greatly increase the complexity of the analysis, at the expense of high computational cost, which both are not very suitable to industrial needs. Furthermore, a complex modelling approach might also hinder the understanding of the basic mechanisms that govern the system thermo-mechanical response, as well as the identification of the relevant design parameters. It is then

desirable to find out a simplified modelling approach, which matches high accuracy and low computational cost.

On the other hand, the results of Appendix A, which will be discussed later in the paper, will clearly show how a transient analysis with phase change is actually not necessary in the computation of thermal stresses, as the highest stresses occur only at the start-up phase, when the PCM is solid, whereas much lower stresses occur when the PCM is liquid. In addition, the thermal analysis presented in the next Section will further confirm how a sequence of steady-state analyses with uniform temperature in the PCM system is a quite good approximation of a transient thermal analysis. This conclusion thus fully justifies the thermo-mechanical analysis developed in the next Sections, which considers the PCM container at different temperatures limited to the range of the start-up phase, where the PCM is solid.

3. THERMAL ANALYSIS

In the start-up and switch-off phases, the thermal response of the system can be modelled as a problem of transient conduction. According to [11], the simplest and most convenient method that can be used to solve transient heating and cooling problems is the lumped capacitance method, which assumes that the temperature of a solid body is spatially uniform at any instant during a transient process.

In order to check the conditions that guarantee a reasonable accuracy of this method, it is necessary to estimate the Biot number Bi of the PCM system, defined as the ratio of internal thermal resistance R_{int} and external thermal resistance R_{ext} (see Figure 2a):

$$\mathrm{Bi} = \frac{R_{\mathrm{int}}}{R_{\mathrm{ext}}} \tag{1}$$

If Bi<0.1, the error associated by using the lumped capacitance method is small and the assumption of uniform temperature within the PCM system can be made with a negligible error.

It has to be considered that the PCM system at the back receives less heat as compared to that at the front area of the arrangement of Figure 1a. Therefore, each PCM system is characterized by a different Biot number. According to the lumped capacitance method, the smaller the Biot number, the more accurate is the assumption of uniform temperature in the body at any time instant. Therefore, only the PCM system with the highest Biot number has to be checked.

The highest Biot number occurs when the internal thermal resistance is maximum R_{int} (i.e. thermal conductivity of the materials is minimum) and the external thermal resistance R_{ext} is minimum (i.e. heat transfer coefficients of the waste gas are maximum).

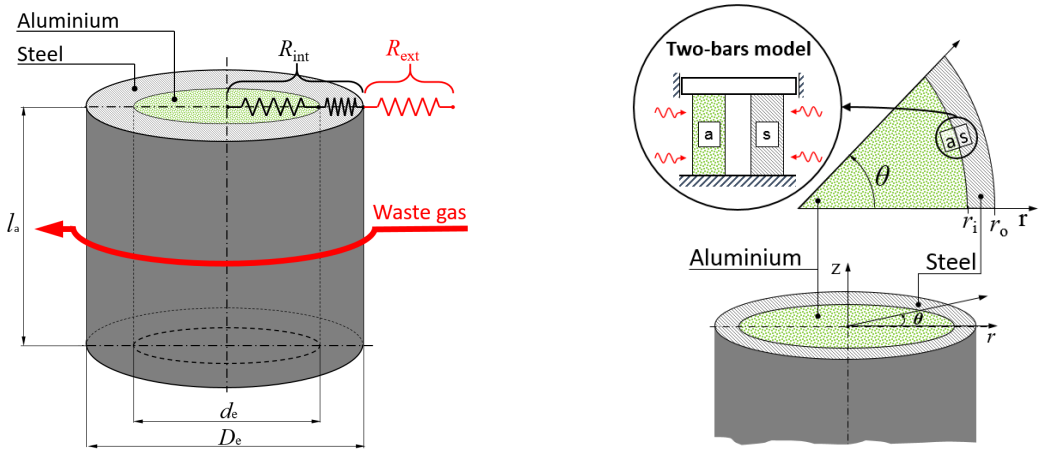

(a) (b)

Figure 2. (a) Thermal model and (b) structural model of the PCM system

The internal thermal resistance R_{int} depends on the resistance to conduction within the materials and the contact resistance at their interface, as expressed in equation (2).

$$R_{\text{int}} = \frac{L_{\text{a}}}{\lambda_{\text{a}}} + \frac{L_{\text{s}}}{\lambda_{\text{s}}} + \frac{1}{h_{if}} \tag{2}$$

where L is a characteristic length associated with the length scale corresponding to the maximum spatial temperature difference, which for the aluminium part is $L_a = d_e/2$ and for the steel part is $L_s = (D_e\text{-}d_e)/2$. Symbols λ_a and λ_s represent the thermal conductivity of aluminium and steel, respectively, while h_{if} represents the interfacial heat transfer coefficient at aluminium/steel interface. In [12], interfacial heat transfer coefficients have been measured for several metal castings in cylindrical steel moulds. In [12], the interfacial heat transfer coefficients have been measured in several metal castings, where melting and solidification occurred in a cylindrical steel mould, exactly as the melting and solidification in the PCM system. Thus, a good estimation of the maximum contact resistance at the aluminium/steel interface in the PCM system can be obtained considering the minimum h_{if} measured in [12], which reports a minimum value of h_{if} =5000 W/m^{2}K for an almost pure aluminium casting in a vertical cylindrical steel mould. The maximum value of R_{int}=5.59E-04 m^{2}K/W results by using the data in Table

2, in which the thermal conductivity of the austenitic stainless steel AISI 316 is used because it is the lowest one among selected steels.

According to equation (3), the external thermal resistance R_{ext} depends on heat transfer coefficients of convection h_{conv} and radiation h_{rad}, which are related to the PCM system arrangement.

$$R_{\mathrm{ext}} = (\, h_{\mathrm{conv}} + \, h_{\mathrm{rad}})^{-1} \tag{3}$$

The thermal analysis considers the PCM system where the heat transfer coefficients are maximum. Estimations carried out in [6] showed that the maximum convection heat transfer coefficient h_{conv} of about 100 W/m^{2}K is achieved in the first row of the PCM system arrangement. As reported in [13], radiation heat transfer coefficient h_{rad} can be estimated as:

$$h_{\mathrm{rad}} = k e_{\mathrm{g}} e_{\mathrm{e}} \chi \frac{T_{\mathrm{g}}^4 - T_{\mathrm{e}}^4}{T_{\mathrm{g}} - T_{\mathrm{e}}} \tag{4}$$

where k is the Stefan-Boltzmann constant, e_g is the emissivity of the waste gas, e_e is the emissivity of the external surface of the PCM system, T_g is the waste gas temperature and T_e is the temperature of the external surface of the PCM system. The dampening factor χ takes into account the influence of dust load; in order to guarantee a conservative calculation, it can be set to 1. Radiation heat transfer is strongly tied to the emission coefficient of the waste gas e_g, which depends on several factors (temperature, chemical composition, total pressure, partial pressure of gas species and domain geometry). In particular, chemical composition is the most important factor that affects e_g. In fact, only absorbing/emitting gases (e.g. water vapour and carbon dioxide) contribute significantly to the radiation heat transfer, while the contribution of nonabsorbing/emitting gases (e.g. nitrogen) is negligible. Waste gas at settling chamber inlet is usually composed by three components: CO_2 (30%), H_2O (20%) and N_2 (50%) [13]. Thus, according to [14], the emission factor of waste gas can be calculated as:

$$e_{\mathrm{g}} = \, e_{CO_2} + e_{H_2O} - \Delta e \tag{5}$$

where Δe is a correction factor which takes into account the overlap of the individual emission bands of the gases involved. For what concerns the emission factor e_e of the external surface of the PCM system, it can be considered very close to 1. Based on the data provided in [6] the maximum heat transfer coefficient of waste gas radiation h_{rad} results equal to 26 W/m^{2}K and, according to eq. (3), the minimum external resistance results R_{ext} = 7.94E-03 m^{2}K/W.

198 The estimated maximum R_{int} and minimum R_{ext} give a maximum Biot number of the PCM system equal
199 to 0.07, which is lower than 0.1. Thus, the internal thermal resistance R_{int} can be neglected and each
200 PCM system can be assumed, with a negligible error, to be at uniform temperature. Since the PCM
201 system has a very small Biot number, the system temperature can be considered almost uniform at any
202 time instant of start-up and switch-off phases. In such phases, the thermal behaviour of PCM system can
203 thus be simulated as a sequence of steady state analyses. The hypothesis of steady-state thermal analysis
204 and uniform temperature distribution in the PCM system, which is used in the thermo-mechanical
205 analysis of the following Sections, has been further justified by the transient numerical simulation
206 presented in Appendix A.
207

208 ## 4. ANALYTICAL MODEL

209 Before facing an elastic-plastic analysis, which will be described in Section 5, it is useful to preliminary
210 evaluate the thermo-mechanical response of the PCM system by a simple linear elastic analysis. An
211 analytical model is then employed to estimate the thermal stress distribution in the PCM system and to
212 identify the most suitable stainless steel for the PCM container.

213 Table 3. Structural properties of the materials [10]-[15]

	Elastic Modulus, E [GPa]							Thermal expansion Coeff., α [10^{-5}/K]	Poisson ratio, ν
Temperature [°C]	*20*	*100*	*200*	*300*	*400*	*500*	*550*	-	-
Aluminium	70	68	60	48	28	14	0	2.3	0.34
AISI 316 - Austenitic	200	192	184	176	168	160	154	1.7	0.3
AISI 410S - Ferritic	220	211	202	194	185	176	172	1.0	0.3

214 According to the conclusions of the thermal analysis in Section 3, the PCM system is at almost uniform
215 temperature at any time instant. No thermal gradient then occurs along the axial direction. This allows
216 the thermo-mechanical behaviour of the system to be studied by a plane model, as shown in Figure 2b.
217 In addition, the axial symmetry of both geometry and thermal loads (i.e. temperature is symmetrical
218 about the centre) allows using the "axialsymmetric plane model" of Timoshenko [16]. This plane model
219 derives the analytical expressions for the radial σ_r and tangential (or hoop) σ_θ stresses. The axial stress
220 σ_z, instead, can range from plane stress $\sigma_z=0$ (free axial thermal expansion) to plain strain condition $\sigma_z\neq0$
221 (totally constrained axial thermal expansion), depending on the axial boundary condition applied to the

PCM system. The plane stress and plain strain conditions are called the "plane circular disk" and "long circular cylinder" in [16].

In the PCM system, however, the axial stress σ_z is also influenced by the mismatch in the axial thermal expansion of aluminium and steel parts, which also gives rise to a shear stress τ_{rz} at the aluminium/steel interface (note, instead, that $\tau_{\theta z}= \tau_{\theta r}=0$ for symmetry). This shear stress τ_{rz} tends to prevent the free sliding, and thus the free axial thermal expansion, of the aluminium part over the steel container (in fact, the aluminium expands more than steel under the same temperature change). The shear stress is, then, also directly influenced by the value of friction coefficient at the aluminium/steel interface.

This complex situation makes difficult to identify which axial boundary condition (plane stress or plane strain), and thus which axial stress σ_z, can reasonably be assumed in the analytical model of the PCM system. An answer is then given by a preliminary numerical study that has been performed by the plane axisymmetric finite element model described in Appendix B. The obtained results, shown in Figure 11, confirmed that the plane stress hypothesis, where the axial stress $\sigma_z=0$, is a reasonable assumption for the analytical model of the PCM system.

In the "axialsymmetric plane model", the general expressions of radial σ_r and tangential σ_θ stresses, as well as radial displacement u, are:

$$\sigma_r(r) = -\alpha E \frac{1}{r^2}\int_a^r \Delta T r dr + \frac{E}{1-\nu^2}\left[C_1(1+\nu) - C_2(1-\nu)\frac{1}{r^2}\right] \quad (6)$$

$$\sigma_\theta(r) = \alpha E \frac{1}{r^2}\int_a^r \Delta T r dr - \alpha E \Delta T + \frac{E}{1-\nu^2}\left[C_1(1+\nu) + C_2(1-\nu)\frac{1}{r^2}\right] \quad (7)$$

$$u(r) = (1+\nu)\alpha \frac{1}{r}\int_a^r \Delta T r dr + C_1 r + \frac{C_2}{r} \quad (8)$$

where r is the radial coordinate, a is the inner radius, E is the elastic modulus, ν the Poisson coefficient and α the coefficient of thermal expansion. The temperature increment is $\Delta T = T(r) - T_{ref}$, where $T(r)$ is the temperature distribution in the body and T_{ref} a reference temperature. In the above equations, symbols C_1, C_2 are unknown parameters that depend on the applied boundary conditions.

Section 3 emphasised that, at each time instant in start-up and switch-off phases, the PCM system can be considered at a uniform temperature, which means that $T(r) = T_\Gamma$ = const. is the system temperature at time instant Γ. The temperature increment is also constant, $\Delta T = T_\Gamma - T_{ref}$.

For the system in Figure 2b, which is formed by two different materials, two sets of three equations must be defined: one set for aluminium, one set for steel. For the part of domain filled with aluminium, it is $a = 0$ (solid disk); the surrounding domain related to the container (steel), it is $a = r_\mathrm{i}$. According to [16], for a solid disk $C_2 = 0$, in order that the displacement $u_\mathrm{a}(r)$ is zero at the centre $r = 0$. Thus, this gives the following expressions:

$$\begin{cases} \sigma_{\mathrm{r_a}}(r) = -\alpha_\mathrm{a} E_\mathrm{a} \dfrac{\Delta T}{2} + \dfrac{E_a}{1-\nu_\mathrm{a}^2}\left[C_{1,\mathrm{a}}(1+\nu_\mathrm{a})\right] \\ \sigma_{\theta_\mathrm{a}}(r) = -\alpha_\mathrm{a} E_\mathrm{a} \dfrac{\Delta T}{2} + \dfrac{E_\mathrm{a}}{1-\nu_\mathrm{a}^2}\left[C_{1,\mathrm{a}}(1+\nu_\mathrm{a})\right] \\ u_\mathrm{a}(r) = (1+\nu_\mathrm{a})\alpha_\mathrm{a}\dfrac{\Delta T}{2} r + C_{1,\mathrm{a}} r \end{cases} \tag{9}$$

$$\begin{cases} \sigma_{r_\mathrm{s}}(r) = -\alpha_\mathrm{s} E_\mathrm{s} \dfrac{\Delta T}{2}\left(1 - \dfrac{r_\mathrm{i}^2}{r^2}\right) + \dfrac{E_\mathrm{s}}{1-\nu_\mathrm{s}^2}\left[C_{1,\mathrm{s}}(1+\nu_\mathrm{s}) - C_{2,\mathrm{s}}(1-\nu_\mathrm{s})\dfrac{1}{r^2}\right] \\ \sigma_{\theta_s}(r) = -\alpha_\mathrm{s} E_\mathrm{s} \dfrac{\Delta T}{2}\left(1 + \dfrac{r_\mathrm{i}^2}{r^2}\right) + \dfrac{E_\mathrm{s}}{1-\nu_\mathrm{s}^2}\left[C_{1,\mathrm{s}}(1+\nu_\mathrm{s}) - C_{2,\mathrm{s}}(1-\nu_\mathrm{s})\dfrac{1}{r^2}\right] \\ u_\mathrm{s}(r) = (1+\nu_\mathrm{s})\alpha_\mathrm{s}\dfrac{\Delta T}{2}\dfrac{r^2 - r_i^2}{r} + C_{1,s} r + \dfrac{C_{2,s}}{r} \end{cases} \tag{10}$$

Equation (7) shows that, in the aluminium domain, the state of stress is plane hydrostatic, as the radial and hoop stresses are equal and also constant in the whole domain.

The remaining three unknown parameters $C_{1,\mathrm{a}}$, $C_{1,\mathrm{s}}$, $C_{2,\mathrm{s}}$ can be determined by imposing the appropriate boundary conditions:

$$\sigma_{\mathrm{r,s}}(r_\mathrm{o}) = 0 \tag{11}$$

$$\sigma_{\mathrm{r,a}}(r_\mathrm{i}) = \sigma_{\mathrm{r,s}}(r_\mathrm{i}) \tag{12}$$

$$u_\mathrm{a}(r_\mathrm{i}) = u_\mathrm{s}(r_\mathrm{i}) \tag{13}$$

The above expressions represent zero radial stress (11) at outer stress-free surface of the domain, the continuity of radial stresses (12) and the continuity of radial displacement (13) at the interface $r = r_\mathrm{i}$.

The conditions in equations (11)-(13), combined with the expressions in equations (9)-(10), allow one to calculate closed-form analytical equations for the parameters $C_{1,\mathrm{a}}$, $C_{1,\mathrm{s}}$, $C_{2,\mathrm{s}}$:

$$C_{1,\mathrm{a}} = \frac{\Delta T(1-\nu_\mathrm{a})\alpha_\mathrm{a}\left\{r_\mathrm{i}^2(1-\nu_\mathrm{s}) + r_\mathrm{o}^2(1+\nu_\mathrm{s}) + [2\psi\xi - \xi(1+\nu_a)]\left(r_\mathrm{o}^2 - r_\mathrm{i}^2\right)\right\}}{2[r_\mathrm{i}^2(1-\nu_\mathrm{s}) + r_\mathrm{o}^2(1+\nu_\mathrm{s})] + \xi(1-\nu_a)(r_\mathrm{o}^2 - r_\mathrm{i}^2)} \tag{14}$$

$$C_{1,\mathrm{s}} = \frac{\Delta T(1-\nu_\mathrm{s})\alpha_\mathrm{a}\left[\psi\xi(1-\nu_a)\left(r_\mathrm{o}^2 - r_\mathrm{i}^2\right) + \psi(1+\nu_\mathrm{s})\left(r_\mathrm{o}^2 - r_\mathrm{i}^2\right) + 2r_\mathrm{i}^2\right]}{2[r_\mathrm{i}^2(1-\nu_\mathrm{s}) + r_\mathrm{o}^2(1+\nu_\mathrm{s})] + \xi(1-\nu_a)(r_\mathrm{o}^2 - r_\mathrm{i}^2)} \tag{15}$$

$$C_{2,\mathrm{s}} = \frac{\Delta T r_\mathrm{i}^2(1+\nu_\mathrm{s})\alpha_\mathrm{a}\left\{[\psi\xi(1-\nu_a) - \psi(1-\nu_\mathrm{s})]\left(r_\mathrm{o}^2 - r_\mathrm{i}^2\right) + 2r_\mathrm{o}^2\right\}}{2[r_\mathrm{i}^2(1-\nu_\mathrm{s}) + r_\mathrm{o}^2(1+\nu_\mathrm{s})] + \xi(1-\nu_a)(r_\mathrm{o}^2 - r_\mathrm{i}^2)} \tag{16}$$

where $\psi = \alpha_s/\alpha_a$ and $\xi = E_s/E_a$ are dimensionless coefficients, which account for the difference in material properties between aluminium and steel. Note that in the hypothesis of same material in the whole PCM system, it is $\psi = \alpha_s/\alpha_a$ and $\xi = E_s/E_a$. Accordingly, the expressions (9)-(10) give a stress $\sigma_{r,a} = \sigma_{\theta,a} = 0$ and $\sigma_{r,s} = \sigma_{\theta,s} = 0$ in the whole domain, which coincides with the results given in [16] for the case of solid cylinder and then confirms the correctness of the previous equations.

The distribution of tangential σ_θ and radial σ_r stress in aluminium and steel container can be computed by expressions (9)-(10) with the coefficients in (14)-(16). The temperature increment $\Delta T = T_\Gamma - T_{ref}$ is calculated by considering the temperature T_Γ at time instant Γ in the start-up or switch-off phase; in this study, the reference temperature is $T_{ref} = 20$ °C. The axial stress is found, instead, by a simple equilibrium condition along the axial direction. In fact, as previously said, the PCM system is free to expand along its axis, thus the axial stress σ_z in the container is only generated by the total weight of the system. Considering the parameters in Table 1, the axial stress is $\sigma_z = 0.5$ MPa and it can be neglected for practical purposes.

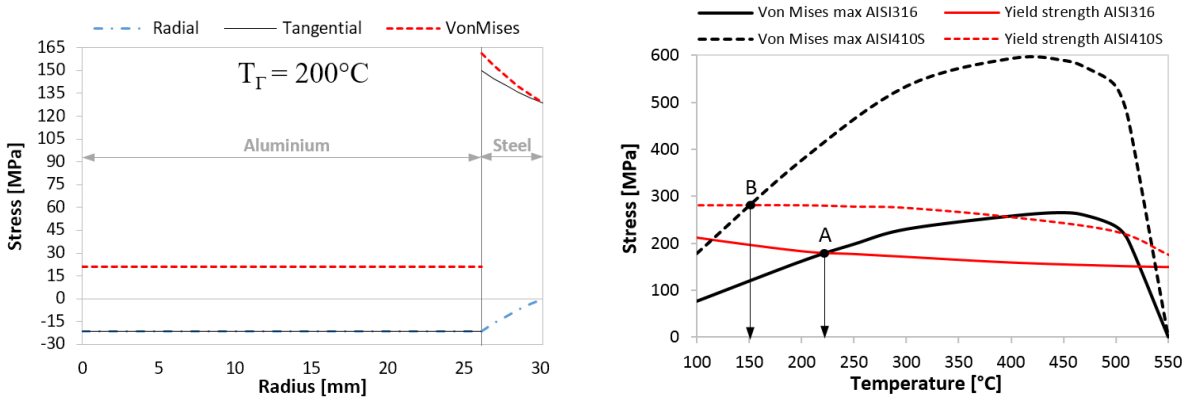

(a) (b)

Figure 3. (a) Example of stress distribution (radial, tangential, Von Mises) in PCM system at temperature T_Γ =200 °C, steel is AISI 316; (b) yield strength (red lines) and maximum Von Mises stress (black lines) at inner radius, as a function of temperature T_Γ, for the two considered stainless steels

Figure 3a reports an example of stress distribution in the PCM system at temperature $T_\Gamma = 200$ °C. The stress distribution in the steel container is similar to that in a cylindrical vessel under internal pressure. The radial stress σ_r is compressive within the whole PCM system; it is constant in the aluminium, continuous at the aluminium/steel interface, while it decreases to zero at the outer radius of the container. The tangential stress σ_θ is also compressive in the aluminium (where it overlaps to radial stress), while it becomes tensile in the steel container (i.e. a discontinuity occurs at aluminium/steel

277 interface). The compressive stresses inside the aluminium are then balanced by the tensile tangential
278 stresses in the steel container. The axial stress σ_z is almost zero in the whole domain.
279 The stress distribution in Figure 3a, which occurs in start-up and switch-off phases, can be explained by
280 the mismatch in mechanical properties of aluminium and steel (e.g. coefficient of thermal expansion and
281 elastic modulus). The aluminium has a coefficient of thermal expansion greater than that of steel, which
282 leads aluminium to expand more than the container. This thermal expansion, however, is hindered by
283 the steel container, because of its much higher elastic modulus at any temperature (see Table 3). The
284 stress distribution then depends on the mechanical properties of the steel grade used for the container.
285 Figure 3a also plots the distribution of the equivalent Von Mises stress:

$$\sigma_{\mathrm{vm}} = \sqrt{\sigma_{\mathrm{r}}^2 + \sigma_{\theta}^2 - \sigma_{\mathrm{r}}\sigma_{\theta}} \tag{17}$$

286 in which the axial stress σ_z has been neglected. The maximum Von Mises stress is located at the inner
287 radius of the steel container, where plastic strain is then expected to occur. This is the most critical point
288 in the PCM system, which has to be monitored in the design. Similarly to the overall stress distribution,
289 also the maximum Von Mises stress depends on the steel type, as shown in Figure 3b.
290 To understand the mechanical behaviour of PCM system during the start-up and switch-off phases, it is
291 of interest to plot the maximum Von Mises stress $\sigma_{\mathrm{vm,max}}$ at each temperature T_Γ reached in such phases
292 (T_Γ = 100÷660 °C).
293 Figure 3b shows that Von Mises stress has a nearly parabolic profile, with a peak around 450°C, where
294 the combination of thermal expansion and mechanical constraint reaches its maximum effect.
295 The analysis also highlights how the Von Mises stress in AISI410S steel is more than double to that
296 generated into AISI316 steel. This stress difference can be explained by considering that AISI410 steel
297 has a lower coefficient of thermal expansion and a higher elastic modulus than those of AISI 316 steel
298 (see Table 3). Figure 3b also compares the maximum Von Mises stress to the yield stress σ_y of each steel
299 type considered as container material; it can be observed that, at any temperature, the AISI 316 steel has
300 a yield stress lower than that of AISI410S steel. Yielding occurs at the temperature T_y where the
301 maximum Von Mises stress $\sigma_{\mathrm{vm,max}}$ reaches the yield stress $\sigma_y(T)$. Figure 3b shows that yielding occurs
302 at T_y = 150°C for the AISI410S (point B) and at T_y = 225°C for the AISI316 (point A). For temperatures

303 $T > T_y$ plastic strain begins and, of course, the Von Mises stress calculated by the elastic model is no
304 longer representative of the state of stress in the container. Therefore, the most suitable stainless steel
305 for the container is AISI 316, because its lower stress levels allow the container to behave elastically
306 over a temperature range wider than that of AISI410S.
307 The mechanism that generates thermal stresses in PCM system can be interpreted and further explained
308 by using the simple two-bars model in Figure 2b, which has been suggested by Manson [17]. This
309 mechanical model exemplifies the tangential (hoop) displacements of two small elementary elements of
310 aluminium and steel, located at the interface between aluminium and steel in the PCM system. The two
311 bars, connected at both ends, expand under a temperature increase ΔT.
312 In the model, the total strain is $\varepsilon_{tot} = \varepsilon_{th} + \varepsilon_{mec}$, where $\varepsilon_{th} = \alpha\ \Delta T$ is the thermal strain for a temperature
313 variation $\Delta T = T_\Gamma - T_{ref}$ and ε_{mec} is the mechanical strain, which is responsible for the stress $\sigma = E\ \varepsilon_{mec}$.
314 In the simplified two-bars model, the amount of thermal strain $\varepsilon_{th} = \alpha\ \Delta T$ is proportional to the
315 temperature change ΔT and to the coefficient of thermal expansion of the material α. The thermal strain
316 induces a thermal expansion of the system, which, however, can be limited partially, depending on the
317 imposed amount of mechanical constraint.
318 A free thermal expansion occurs when no mechanical constraint is imposed, which in turn gives no
319 mechanical strain and stress in the system. The amount of mechanical constraint imposed on thermal
320 strain depends, of course, on the mechanical stiffness of the system (e.g. elastic modulus and geometry).
321 It is then clear that the mechanical strain ε_{mec} (which generates the stress) depends on the relative
322 contribution of thermal expansion and imposed mechanical constraint. Two limiting cases exist: i) free
323 thermal expansion with no mechanical constraint (which gives a stress-free situation) and ii) totally
324 constrained thermal expansion (which gives rise to the maximum stress). In the case of no mechanical
325 constraint on thermal expansion, the total strain equals the thermal strain $\varepsilon_{tot} = \varepsilon_{th}$ and the mechanical
326 strain is zero $\varepsilon_{mec} = 0$, with no stress on the system; this situation describes the free thermal expansion
327 without any mechanical stress. Conversely, in the case of totally constrained thermal expansion, the total
328 strain is zero $\varepsilon_{tot} = 0$ and all the thermal strain is converted into mechanical strain $\varepsilon_{mec} = -\varepsilon_{th} = -\alpha\Delta T$,
329 which then becomes directly proportional to the temperature variation (the higher the temperature, the
330 higher the stress).

In the PCM system, both aluminium and steel container tend to expand for an imposed temperature variation. The constraint on the free thermal expansion of the aluminium is imposed by the surrounding steel container; this constraint, however, is partially relaxed by the thermal expansion of the steel container itself. On the other hand, the imposed constraint also depends on the stiffness (i.e. elastic modulus) of both materials, which in turn decreases with temperature. A result, the PCM system is in a halfway condition between the two limit cases explained above and the amount of thermal stress depends on several parameters of the PCM system, as well as on temperature.

The governing equations of the two-bars model and the resulting thermal stresses are derived in Appendix C. Based on the stress equations (C.4) and (C.5), all the relevant parameters that control the amount of thermal stress in the steel container can be conveniently summarised in the following stress index:

$$i = \frac{(\alpha_a - \alpha_s)\Delta T}{1 + \xi} \tag{18}$$

which is obtained from the expression (C.5) by assuming an equal area ($A_a = A_s$) for the two bars. In expression (18), $\Delta T = T_\Gamma - T_{ref}$ is the imposed temperature variation, α_a, E_a and α_s, E_s are, respectively, the coefficient of thermal expansion and elastic modulus for aluminium and steel, evaluated at temperature T_Γ.

The assumption of equal area is justified by considering that the two-bars model represents two small elementary elements (see Figure 2b) of same geometry: this allows the index i to evaluate the effect of material properties on the coupling at the interface, regardless of the particular geometry of the PCM system.

The stress index i can provide a simple, although approximate, estimate of the severity of thermal stresses that could develop in the PCM steel container, depending on the materials used. The higher the index i, the higher the thermal stresses expected in the system. An index $i = 0$ means that no thermal stress would develop in the steel container.

Quite intuitively, the stress index i is proportional to the difference (α_a - α_s) in thermal expansion coefficients, to quantify that thermal stress is proportional to the mismatch in thermal strain that occurs in different materials subjected to the same temperature change ΔT. The higher the difference (α_a - α_s)

357 is, the higher the thermal strain mismatch and thus the resulting thermal stresses. If both materials had
358 identical thermal strains (which occurs when $\alpha_a = \alpha_s$), the stress index would be $i = 0$ and no stress would
359 virtually develop in the system, irrespective of the values of the elastic moduli E_a, E_s of both materials.
360 The stress index i also depends on the ratio $\xi = E_s/E_a$, to quantify that thermal stress depends on the
361 mechanical constraint imposed on thermal strain.
362 The ratio ξ is also a function of temperature. For example, when aluminium approaches its melting
363 temperature $T_{m,a}$, its elastic modulus E_a becomes so small compared to E_s, that the ratio ξ diverges to
364 infinity and the stress index $i \rightarrow 0$, with no stress in the steel container (see Figure 4). Conversely, at
365 lower temperature the ratio ξ is higher, which means that steel container is so stiff to prevent the thermal
366 expansion of the contained aluminium, and a higher thermal stresses develop, see Figure 4.

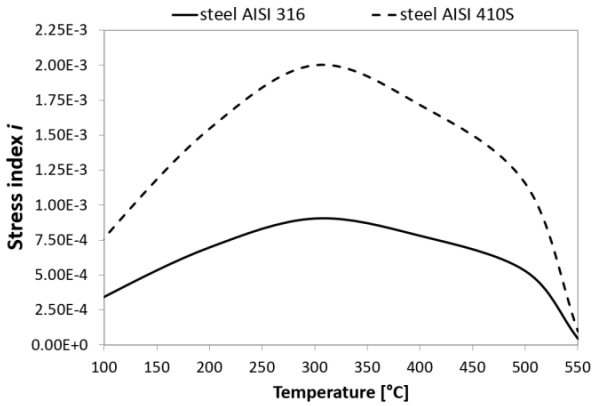

Figure 4. Comparison of the stress index i for the steels AISI 316 and AISI 410S.

367 Owing to its simple expression, the stress index i can be very useful for a sensitivity analysis on materials
368 properties, which allows a preliminary comparison among different materials in the choice of the best
369 material for the PCM container. As an example, Figure 4 shows the comparison of the stress index i
370 calculated for the AISI316 and AISI 410S steels, with the materials properties in Table 3. The similarly
371 of the trends in Figure 4 with the results in Figure 3 is evident, which confirms the validity of the two-
372 bars model.
373

374 ## 5. ELASTIC-PLASTIC MODEL

375 The results in the previous section has shown that the stresses in the container exceed the yield point of
376 the considered steels for temperature higher than 120°C for the AISI410S and higher than 200°C for

377 AISI316 respectively. An elastic-plastic model of the container is then required to study the behaviour
378 of the component during the whole start-up phase and to estimate the extension of the plastic zone.
379 The finite element method is used to analyse the thermo-mechanical elastic-plastic behaviour of the thin
380 circular disk model. The results of the elastic model identified the AISI 316 steel as the most suitable
381 containment material among the considered steels and justified the hypothesis of plane stress, which can
382 thus be employed also in the elastic-plastic model.
383 The one quarter finite element model, shown in Figure 5a, adopts 4-nodes isoparametric linear elements
384 to discretise both aluminium and steel parts. A mapped mesh is used for the container domain and the
385 aluminium close to the interface, a free mesh is used elsewhere. The thermal analysis is first carried out
386 to compute the temperature in each node; the calculated nodal temperatures are then input as thermal
387 loads in the next mechanical analysis.
388 A numerical uncertainly analysis has initially been performed to assess the approximation errors of the
389 finite element solution. In particular, a convergence analysis on the element size has been carried out to
390 identify at which element size the solution of the finite model in Figure 5(a) becomes grid independent.
391 On the other hand, it has to be noted that the model has a very simple geometry (without notches or
392 geometrical discontinuities), that a refined mesh is not necessary. Subsequently, the correctness of the
393 finite element solution has also been verified by comparison with the results of the theoretical model of
394 Section 4 (an error of less than 1% was observed, which is fully acceptable). Unfortunately, a
395 comparison with experimental data is not possible, as to our knowledge experimental data for this type
396 of PCM configuration are not available.
397 As evidenced in Section 3, it is possible to consider the system at uniform (steady state) temperature at
398 any given time instant. This consideration allows simulating the thermo-mechanic behaviour of the
399 component by a sequence of steady state analyses. In the thermal analysis, the applied thermal load is
400 simply a uniform temperature on the whole finite element model. In the mechanical analysis, symmetry
401 boundary conditions are applied as shown in Figure 5a; the hypothesis of plane stress is considered. An
402 elastic-perfectly plastic material model has been used for aluminium and steel. A small positive value
403 of the hardening modulus has been set to obtain convergence of the numerical solution. All thermal and
404 mechanical properties are considered to be temperature dependent, as in Table 3.

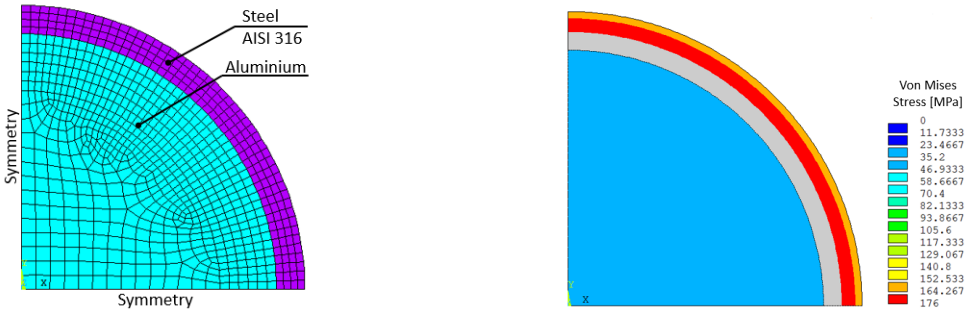

(a) (b)

Figure 5. (a) Finite element model and (b) plastic strain (grey colour) of the container at 250 °C

Figure 5b shows the Von Mises stress distribution; the colour scale is bounded by the value of the yield stress of AISI316 stainless steel at 250°C. Therefore, the grey colour represents the region where plastic strain occurs, while the remaining parts are only subjected to elastic strain. Figure 6a reports the profile of the Von Mises stress distribution of Figure 5b along a radial direction; the distribution of radial, tangential and axial stresses are also shown. The trends in Figure 6a are actually similar to those in Figure 3a. In the elastic-plastic results, however, a lower tangential stress σ_θ is observed at the inner radius, where the maximum Von Mises stress is equal to the yield stress.

The comparison between the Von stress calculated by the FEM model and the elastic analytical model is reported in Figure 6b. In particular, the maximum Von Mises stress at the inner radius r_i and the Von Mises stress at the outer radius r_o of the container are reported in Figure 6b; the yield stress of the stainless steel AISI 316 is also shown.

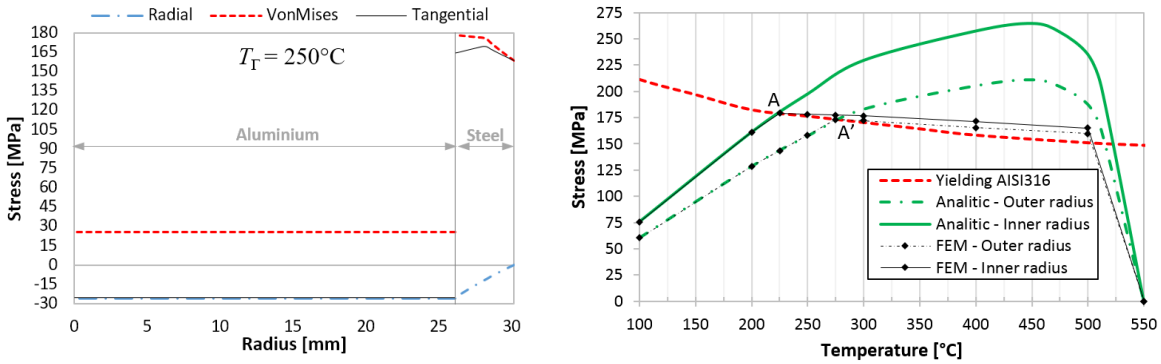

(a) (b)

Figure 6. (a) Stress distribution as radius function and (b) comparison between Von Mises stress distribution of the elastic analytical model and the elastic-plastic FEM model

Figure 6b shows that the plastic deformation of the container starts at 225 °C (point A) from the inner radius and it expands along radial direction as the temperature increases; the complete plastic

deformation of the whole thickness is reached at 275°C (point A'). In the elastic-plastic model, a preliminary evaluation of component structural integrity can be performed by comparing the maximum elastic-plastic strain to the material fracture strain. The graph in Figure 6b allows considering that at a temperature of about 500 °C the maximum elasto-plastic strain is 1.79e-3, which is far below the fracture strain $\varepsilon_f = 0.4$ of AISI316 at 500 °C [10]. It can be concluded that the component can resist to a single phase of start-up.

6. ALTERNATIVE DESIGN OF PCM CONTAINER

The previous analysis highlighted that the proposed PCM container geometry, sketched in Figure 1b, leads to plastic deformation of the considered steel. However, it is desirable to individuate a PCM container geometry that allows the steel to work within the elastic field. The design of the alternative configuration has also to be as simple as possible to guarantee a low manufacturing cost.

The proposed alternative configuration (Figure 7a) consists of two concentric cylindrical containers (pipes) in stainless steel AISI316, where the hollow cavity is filled by PCM.

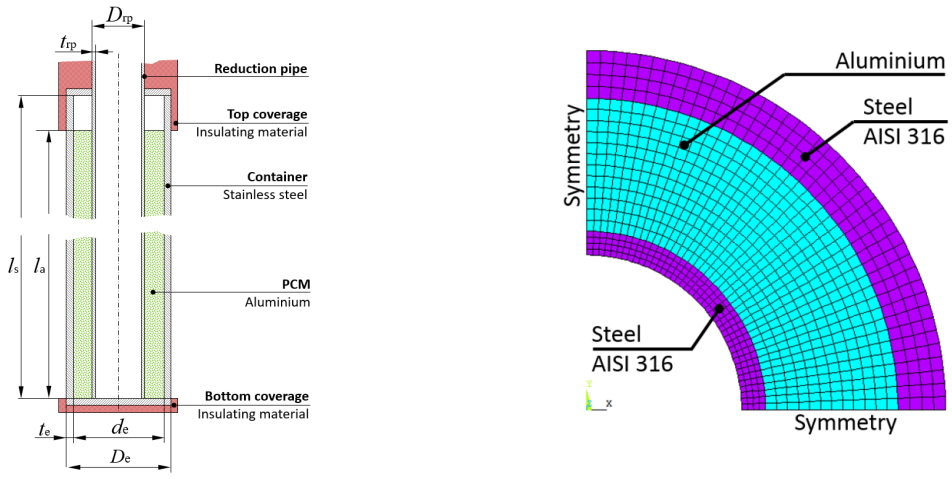

(a) (b)

Figure 7. (a) Alternative configuration with concentric pipes and (b) its finite element model

For a sake of comparison, the diameter of the external pipe is maintained equal to the diameter $D_e = 60.3$ mm of the initial configuration. The internal pipe is named as *reduction pipe*, as its purpose is to reduce the volume available to PCM, and it can be used to hang the container to the settling chamber roof. The dimensions of the reduction pipe (outer diameter and thickness) are design parameters that are investigated by a sensitivity analysis. The new geometrical configuration is studied by exploiting the

elastic-plastic finite element model developed in Section 5. A mapped mesh is now used in the whole domain (see Figure 7b).

First, a sensitivity analysis by varying the diameter of the reduction pipe, in the range D_{rp} = 20÷40 mm, has been carried out, to find that diameter that allows the steel of the external pipe to work within the elastic field. In the sensitivity analysis, the reduction pipe has a thickness t_{rp} = 2 mm, while the external pipe maintains the same thickness t_e = 4 mm of the initial configuration of Figure 1b.

Figure 8a shows the maximum Von Mises stress as a function of temperature, for different values of diameter D_{rp} of the reduction pipe; the yield stress of AISI 316 is also reported. For diameters D_{rp} < 30 mm, plastic deformation still occurs in steel of the external pipe; for diameters D_{rp} > 30 mm, instead, yielding does not occur at any temperature and the steel of the external pipe works in the elastic field. For each diameter D_{rp} > 30 mm, Figure 8a allows individuating the temperature at which the maximum Von Mises stress is reached in the elastic domain; this temperature is defined as "critical temperature" T_{crit} and, for all diameters, it is equal to 400 °C.

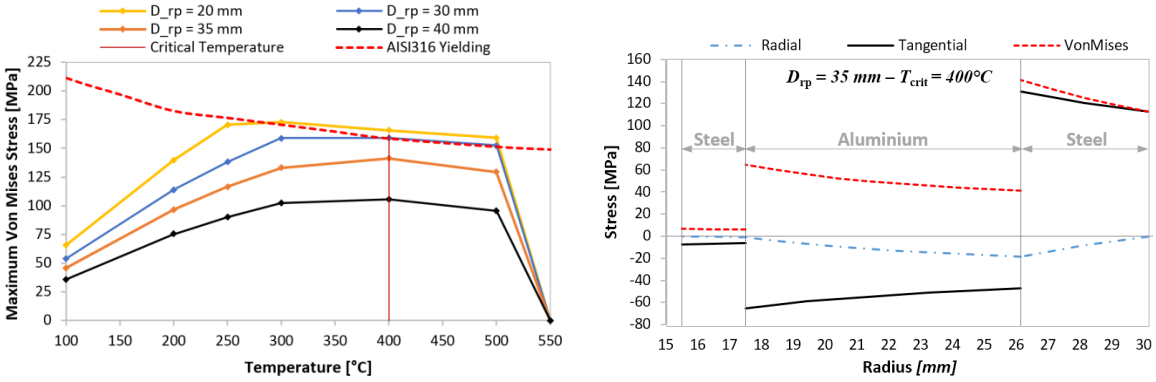

(a) (b)

Figure 8. (a) Maximum Von Mises stress at different temperature and reduction diameter D_{rp}; (b) stress distribution as a function of radius, for D_{rp} =35 mm and T_{crit} = 400 °C

Figure 8b reports the stress distribution in the configuration with diameter D_{rp} = 35 mm, at the critical temperature T_{crit} = 400 °C. It can be seen that the maximum stress is located at the interface between the PCM and the external pipe, while the stress in the reduction pipe is negligible.

The previous analysis has shown that the reduction pipe becomes a fundamental element of the PCM system as it allows the steel to work within the elastic field. A further sensitivity analysis at the critical temperature 400 °C has been carried out by varying the thickness t_{rp}, t_e of the reduction pipe and external pipe.

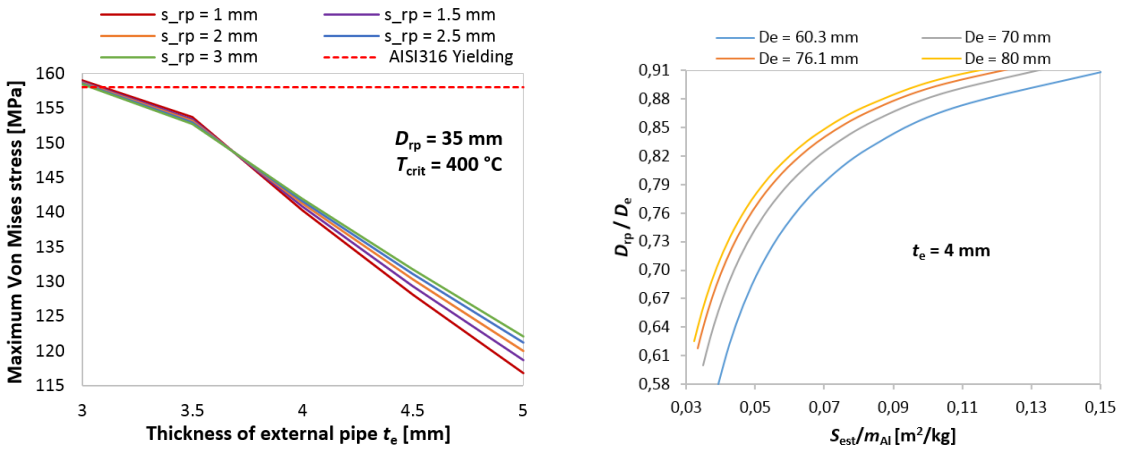

(a) (b)

Figure 9. (a) Sensitivity analysis by varying reduction pipe t_{rp} and external pipe t_e thickness and (b) possible configuration as function of the ratio A_{est}/m_{Al} and of D_e to t_e = 4 mm

Figure 9a shows an example of sensitivity analysis for the configuration with diameter D_{rp} = 35 mm of the reduction pipe. The plot shows that the thermal stress is mainly influenced by the thickness t_e of the external pipe, while the effect of the thickness t_{rp} of reduction pipe is actually negligible.

The smallest thickness t_{rp} = 1 mm of the reduction pipe is chosen as it gives the lighter weight of the structure while assuring low stresses (axial stress due to the component weight σ_z< 0.5 MPa and stress generated by the aluminium expansion $\sigma_{vm,max}$ < 10 MPa). The thickness of 1 mm has then been used as a reference value to define the "allowable configurations", which are all the geometrical configurations where the container works in the elastic field.

The design of the whole PCM system is first based on thermo-physical parameters, mainly represented by the ratio of external surface of heat exchange A_{est} to the aluminium mass m_{Al}. Figure 9b shows an example of allowable configurations for the external thickness t_e = 4 mm in terms of diameter ratio D_{rp} /D_e and as a function of the ratio A_{est}/m_{Al}. Figure 9b shows a typical design chart to identify the allowable configurations; in particular, the figure reports the diameter ratio D_{rp} /D_e as a function of A_{est}/m_{Al} for a given external thickness t_e=4 mm and for different external diameters D_e.

7. CONCLUSIONS

This article presented an analytical and numerical approach to evaluate thermal stress in a phase change material (PCM) system, used for temperature smoothing of waste gas of Electric Arc Furnace. Thermal analysis showed that the Biot number of the PCM system is less than 0.1 and therefore the PCM system

can be assumed, with a negligible error, to be at uniform temperature at any time instant. This isothermal condition allowed the thermo-mechanical behaviour of the system to be simulated by a sequence of steady-state analyses.

The mechanical analysis based on axialsymmetric plane analytical model allowed to compare elastic thermal stress distribution for AISI410S and AISI316 stainless steels and to identify the latter as the most suitable material for the PCM container. The simple two-bars model and a stress index are used to explain the thermal stress distribution in the PCM system and the nearly-parabolic profile of Von Mises stress over temperature. Mechanical analysis showed that thermal stresses exceed the yield point of both stainless steels used in the container. Therefore, a FEM analysis has been carried out to evaluate the elastic-plastic behaviour of the component. The results showed that a total plastic deformation of the container can occur even during a single start-up phase, where the PCM system is heated from room temperature up to the melting point of PCM. An alternative geometrical configuration with concentric cylindrical containers (pipes) has finally been designed to avoid plastic deformation in the steel container. A sensitivity analysis on some design parameters allowed identifying diameter of the reduction pipe D_{rp} and thickness of the external pipe as the main design parameters that control the amount of thermal stress in the PCM system.

8. APPENDIX A – TRANSIENT THERMO-MECHANICAL SIMULATION OF PCM SYSTEM RESPONSE

This Appendix presents the distribution of temperature and thermal stresses calculated by a transient thermo-mechanical simulation, which also includes the phase change (melting) of the PCM. The purpose of this simulation is to confirm how the hypothesis of steady state analysis and uniform temperature distribution in the PCM system is a very good approximation of transient analysis. Secondly, the simulation results will also show how the modelling of phase change of PCM is actually not necessary in the computation of thermal stresses, as the highest stress occurs only at the start-up phase when the PCM is solid, whereas much lower stresses occur when the PCM is liquid, or even when it is still solid at temperatures far below the melting point.

The transient thermo-mechanical simulation adopts the same mesh distribution used in the one quarter finite element plane model of Figure 5a, although 8-nodes elements are preferred here to improve solution accuracy. The model is under 'plane stress' condition (i.e. zero axial stress), which is also justified in Appendix B. In transient simulations, thermal analysis is carried out first to compute the time-varying temperature in each node, which is next applied as a load thermal input in the mechanical analysis.

In thermal analysis, to replicate as close as possible the operating condition in the settling chamber (see Figure 1a), the PCM system is subjected to a convection boundary condition, with a film coefficient h_{ext} = 126 W/m^{2}K and a waste gas temperature (bulk temperature) that increases linearly from 200 °C to 950 °C over a time interval of 20 min, then back to 200 °C over the next 20 min, and then kept constant over the final 20 min.

The phase change (melting) of the PCM (aluminium) is simulated by defining an enthalpy vs. temperature curve, which increases by the latent heat H_a=396 kJ/kg (see Table 2) at the melting temperature.

In mechanical simulation, an elastic material model is used, with temperature-dependent mechanical properties as per Table 3; note how the elastic modulus of the PCM (aluminium) rapidly goes to zero for temperatures approaching 660 °C (for example, from 20 °C to 400 °C the elastic modulus is halved).

In simulations the AISI 316 steel is used for the container, but similar conclusions would be obtained by using AISI 410S as well.

In transient simulation, a Newmark time integration scheme is adopted, with a very small integration time step to assure numerical convergence.

Figure 10 shows the temperature and stress over time, monitored at four different locations in the PCM system: i) outer surface of steel container (labelled 'surface'), ii) inner surface of steel container, at the PCM/steel interface (labelled 'interface'), iii) at a point in PCM part, 4 mm underneath the PCM/steel interface (labelled 'sub-interface'), iv) at the centre of PCM.

Figure 10a shows that the temperature distribution within the PCM systems is almost uniform at any time instant (the four lines in the graph are overlapped). Melting of PCM starts after about 20 minutes and lasts for about 18 minutes; the temperature of PCM system then decreases as the bulk temperature goes down to 250 °C. It can be concluded that the hypothesis of uniform temperature distribution within the PCM system is fully justified by the results of transient thermal analysis shown in Figure 10a.

Figure 10b shows the change over time of radial and tangential (hoop) thermal stresses at some locations in the PCM system. The radial stress at 'surface' is always zero, as expected. For more clarity, the graph does not show the lines of radial σ_r and hoop σ_θ stresses at 'centre' and 'sub-interface' locations, because they are practically overlapped to the radial stress σ_r at 'interface', which is compressive in the time intervals 0÷15 min and 38÷60 min (while it is almost zero elsewhere). In the same time intervals where σ_r is compressive, tensile hoop stresses are observed at 'surface' and 'interface' locations. Finally, the graphs in Figure 10b also shows the change over time of Von Mises stress at 'interface' locations, as calculated by Eq. (17).

The results of Figure 10b show the following important findings. The Von Mises stress has a maximum after about 11 min, when the PCM system is at 400 °C and the PCM is still in solid phase, see Figure 10a (melting only starts after 20 min). The maximum Von Mises stress is slightly higher than 250 MPa, which is a value in close agreement to the estimation in Figure 3b given by the analytical model of Section 4.

For time values larger than 11 min, the Von Mises stress (as all other stress components) rapidly decrease; they become almost zero at about 15 min (i.e. when the PCM is still in solid phase). This sharp

548 decrease of stress is explained by the drop in elastic properties of PCM material, which at temperatures
549 above 400 °C actually has a very low value of its elastic modulus (see Table 3). Negligible stresses are
550 then maintained up to 18 min (when melting of PCM starts) and later on, up to 38 min (when the PCM
551 comes back to solid state). The results in Figure 3b then show that melting of PCM actually does not
552 contribute in an increase in calculated stresses, as compared to the values estimated by the analytical
553 model in Section 4.

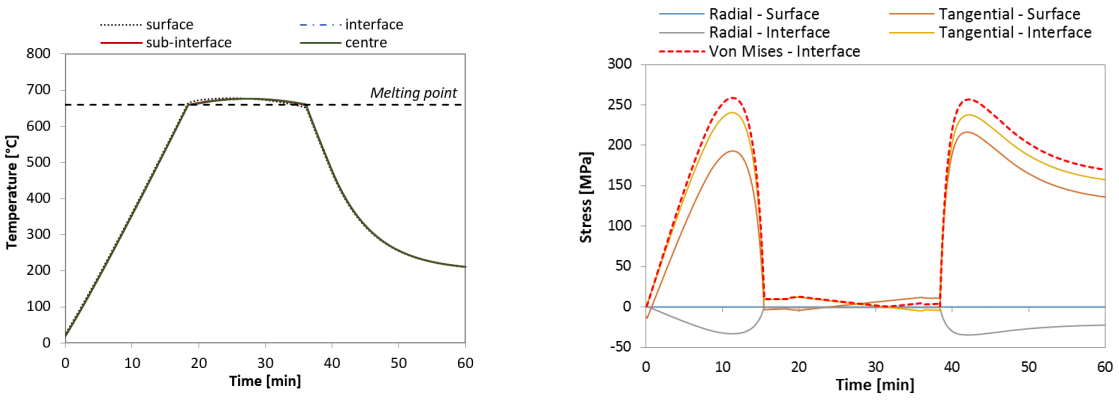

(a) (b)

Figure 10. Results of transient numerical analysis with melting of PCM, monitored at four different locations in the PCM system: (a) temperature evolution; (b) stresses.

554

555 ## 9. APPENDIX B – NUMERICAL STUDY WITH A PLANE AXISYMMETRIC MODEL

556 A small longitudinal portion of the PCM system in Figure 1(b) is analysed by a plane axisymmetric
557 finite element model. Both aluminium and steel regions are discretised by 4-nodes elements with
558 axisymmetric option, arranged in a mapped mesh over the whole domain. Contact elements are also
559 placed at the interface between aluminium and steel container, to simulate the separation and then to
560 allow a relative sliding between the two materials. Two values of the friction coefficient μ were used to
561 simulate two limiting situations: μ=0 for perfect sliding (i.e. no constraint to aluminium thermal
562 expansion), μ=0.65 (a typical value for aluminium/steel coupling) to simulate a constrain to thermal
563 expansion of aluminium. Both aluminium and steel materials are assumed to be linear elastic, with
564 mechanical properties listed in Table 2.
565 The whole model is subjected to a uniform temperature increase (to simulate the start-up phase described
566 in Section 2), which induces a thermal expansion of the contained aluminium. Figure 11 shows the

distribution of stresses (radial σ_r , hoop σ_θ , axial σ_z and shear τ_{rz}) resulting from the analyses with the two values of friction coefficient. The figures also compare the equivalent Von Mises stress:

$$\sigma_{vm} = \sqrt{\sigma_r^2 + \sigma_\theta^2 + \sigma_z^2 - \sigma_r\sigma_\theta - \sigma_r\sigma_z - \sigma_\theta\sigma_z + 3\tau_{rz}^2} \quad \text{(B.1)}$$

to the von Mises stress calculated by Eq. (17) under the plane stress hypothesis (σ_z=τ_{rz}=0).

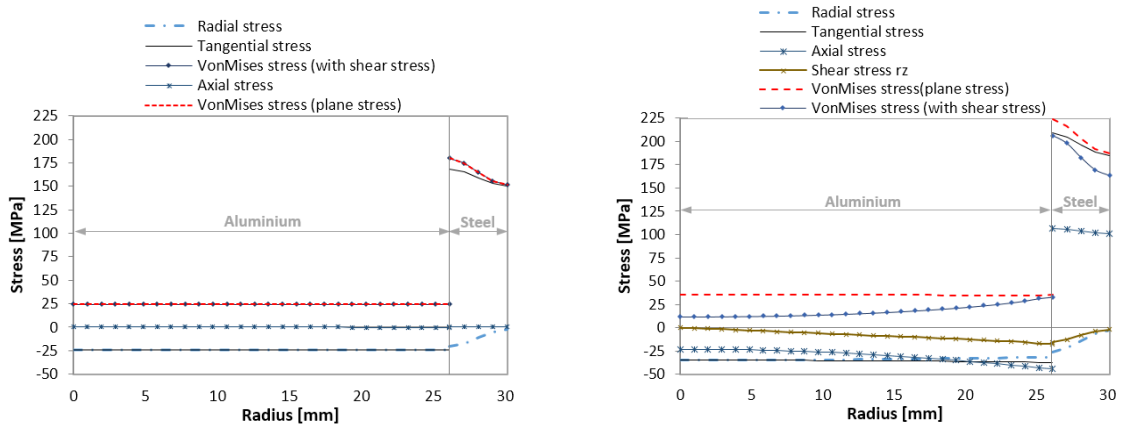

(a) (b)

Figure 11. Stress distribution as a function of radial coordinate for two values of friction coefficient at the aluminium/steel interface: (a) zero friction (μ=0); (b) μ=0.65.

With no friction at the interface (μ=0), there is no constraint to thermal expansion and only radial σ_r and hoop σ_θ stresses develop, while, as expected, the axial and shear stresses are zero (σ_z=τ_{rz}=0). Instead, with a high friction coefficient (μ=0.65) the free thermal expansion of aluminium is prevented and both axial σ_z and shear stress τ_{rz} appear, along with radial σ_r and hoop σ_θ stresses. In aluminium the axial stress is compressive, while it is discontinuous at the interface and then tensile in the steel. The figures show that the axial stress has a small influence on the von Mises stress in the steel container. At the inner radius, the equivalent von Mises stress under plane stress, see Eq. (17), is about 14% higher than the von Mises stress of Eq. (B.1), which considers instead all stress components. Remarkably, the plane stress model is then over-conservative. As known from the theory of strength of materials, there would actually be no difference in equivalent stresses, if they were calculated by using the Guest-Tresca criterion (i.e. maximum shear stress), which computes the equivalent stress σ_{gtr}=| σ_θ – σ_r | as the difference of maximum principal stresses.

These results allow one to conclude that the plane stress hypothesis is a reasonable assumption for the analytical model of the PCM system.

10. APPENDIX C – SIMPLE TWO-BARS MECHANICAL MODEL

The two-bars model in Figure 2b exemplifies two elementary elements at the aluminium/steel interface in the PCM system. The two elements are attached at two rigid plates at both ends. One end plate is fixed, while the plate at the opposite side can translate. No rotations are allowed and the bars can only deform along the longitudinal direction (i.e. this is a one-dimensional model). The two bars, which represent aluminium and steel, have, respectively, areas A_a, A_s , elastic modulus E_a, E_s and coefficient of thermal expansion α_a, α_s. Both bars are subjected to a temperature increment $\Delta T = T\text{-}T_{ref}$, with respect to a reference temperature T_{ref}.

The thermal expansion of the system is partially constrained by the different longitudinal elongation of the two bars, which are then subjected to thermal stresses. The value of thermal stresses can be computed analytically by the expressions.

The total strain in each bar is the sum of thermal strain and mechanical strain:

$$\varepsilon_{tot} = \varepsilon_{th} + \varepsilon_{mec} \tag{C.1}$$

Thermal strain is caused by the temperature increase, $\varepsilon_{th}=\alpha\Delta T$, while the mechanical strain ε_{mec} gives the thermal stress $\sigma=E\varepsilon_{mec}$. The response of the two-bar model in Figure 2b is governed by the following equations (equilibrium and compatibility):

$$\begin{cases} \varepsilon_{tot,a} = \varepsilon_{tot,s} \\ \sigma_a A_a + \sigma_s A_s = 0 \end{cases} \tag{C.2}$$

The first equation states that the elongations of both bars must be equal, because the bars are attached to the same rigid end plate; the second equation specifies the equilibrium of forces transmitted by the two bars to the top rigid plate. By using Eq. (C.1), the first of previous equations can be rewritten as:

$$\alpha_a \Delta T + \frac{\sigma_a}{E_a} = \alpha_s \Delta T + \frac{\sigma_s}{E_s} \tag{C.3}$$

After rearranging, and by using the second equation in (B.2), the stress in the steel bar is obtained as:

$$\sigma_s = \frac{(\alpha_a - \alpha_s) E_s \Delta T}{1 + \frac{E_s A_s}{E_a A_a}} \tag{C.4}$$

while the stress in the aluminium bar is:

$$\sigma_a = -\frac{(\alpha_a - \alpha_s) E_a \Delta T}{1 + \frac{E_a A_a}{E_s A_s}} \tag{C.5}$$

Equations (C.4) and (C.5) show that thermal stresses are directly proportional to the temperature change and, of course, no stress would develop without a temperature variation ($\Delta T = 0$). No stress is also generated (even with a temperature change $\Delta T \neq 0$) if both materials have identical thermal expansion coefficients ($\alpha_a = \alpha_s$), because the two bars elongate with identical thermal expansions. For the aluminium/steel system (where $\alpha_a > \alpha_s$), the equations (C.4)-(C.5) correctly predict a tensile stress in the steel bar and a compressive stress in the aluminium bar, as also shown by the results in Figure 3.

Equations (C.4) and (C.5) also show that thermal stress is controlled by the stiffness values of aluminium and steel elements (summarised by the elastic moduli E_a, E_s), other than by the relative ratio of stiffness (summarised by the ratios E_a/E_s and E_s/E_a).

AKNOWLEDGMENTS

The authors wish to thank Dr. Luciano Moro, University of Udine, for helpful and fruitful discussions on the modelling of transient thermo-mechanical analysis discussed in Appendix A.

REFERENCES

[1] European Commission, Action Plan for a competitive and sustainable steel industry in Europe, 2013

[2] Kirschen M, Risonarta V, Pfeifer H. Energy efficiency and the influence of gas burners to the energy related carbon dioxide emissions of electric arc furnaces in steel industry. Energy 2009; 34:1065–72. DOI:10.1016/j.energy.2009.04.015.

[3] Remus R, Roudier S. Best Available Techniques (BAT) Reference Document for Iron and Steel Production (Integrated Pollution Prevention and Control). 2013. DOI:10.2791/97469.

[4] Born C, Granderath R. Benchmark for heat recovery from the offgas duct of electric arc furnaces. MPT International 2013; 01:32–35.

[5] JP Steel Plantech Co., Green Business Department. Waste Heat Recovery for EAF, http://www.jase-w.eccj.or.jp/technologies/pdf/iron_steel/S-04.pdf, last access May 2015.

[6] Nardin G, Meneghetti A, Dal Magro F, Benedetti N. PCM-based energy recovery from electric arc furnaces. Applied Energy 2014; 136:947-955. DOI:10.1016/j.apenergy.2014.07.052.

[7] Maruoka N, Akiyama T. Thermal Stress Analysis of PCM Encapsulation for Heat Recovery of High Temperature Waste Heat. Journal of Chemical Engineering of Japan 2003; 36(7):794–98. DOI:10.1252/jcej.36.794

[8] Parrado C, Cáceres G, Bize F, Bubnovich V, Baeyens J, Degrève J, Zhang HL. Thermo-Mechanical Analysis of Copper-Encapsulated NaNO3–KNO3. Chemical Engineering Research and Design 2015; 93:224–231. DOI:10.1016/j.cherd.2014.07.007

[9] Blaney JJ, Neti S, Misiolek WZ, Oztekin A. Containment Capsule Stresses for Encapsulated Phase Change Materials. Applied Thermal Engineering 2013; 50(1):555–561. DOI:10.1016/j.applthermaleng.2012.07.014.

[10] EN 1993-1-2:2005 - Eurocode 3 - Design of steel structures Part 1-2: General rules – Structural fire design.

[11] Incropera FP, De Witt DP, Bergman TL, Lavine AS. Fundamentals of Heat and Mass Transfer. vol. 40. 2007.

[12] Bertelli F, Brito C, Meza ES, Cheung N, Garcia A. Inward and outward solidification of cylindrical castings: The role of the metal/mold heat transfer coefficient. Mater Chem Phys 2012;136:545–54. doi:10.1016/j.matchemphys.2012.07.024.

[13] Kirschen M, Velikodorov V, Pfeifer H. Mathematical modelling of heat transfer in dedusting plants and comparison to off-gas measurements at electric arc furnaces. Energy 2006;31:2926–39. doi:10.1016/j.energy.2005.12.006.

[14] VDI Heat Atlas (2° Edition). Springer 2010. DOI: 10.1007/978-3-540-77877-6

[15] EN 1999-1-2:2007 - Eurocode 9 - Design of aluminium structures - Part 1-2: Structural fire design.

[16] Timoshenko S, Goodier JN. Thermal Stress. Theory Elast., New York, NY: McGraw-Hill Book Company; 1951, p. 399–437.

[17] S.S. Manson. Thermal stress and low-cycle fatigue. McGraw-Hill, 1966.